Signal propagation in diffusive molecular communications over a spherical surface

Article (Accepted Version)

Signal Propagation in Diffusive Molecular Communications Over a Spherical Surface

Mengüç Öner, *Member, IEEE,* Esra Sorgüven.

***Abstract*—Diffusive molecular communications (DMC) relies on the Brownian motion of dedicated molecules for transmitting information. The signal propagation characteristics in a DMC channel is determined by the geometries of the environment, receiver and the transmitter and their physical and chemical properties, which impose the boundary- and initial conditions on the partial differential equation (PDE) describing the diffusion process. In this work, we investigate the directional signal propagation characteristics for a point source over (or, as a special case, on) a spherical surface, that may be reflective, perfectly absorptive or partially absorptive. We derive the general solution of the PDE for this case, and validate it via particle based simulations. Our results can be employed to determine the signal propagation characteristics in a wide range of practically relevant scenarios, for which we investigate the effect of the system parameters on the directivity of the signal propagation.**

***Keywords*—Molecular Communications, propagation pattern.**

I. Introduction

The characterisation of signal propagation is an essential step in the design and analysis of a diffusive molecular communication (DMC) system. The position of a single diffusing molecule is a random process with a time-varying probability density function (pdf) satisfying the convection-diffusion-reaction equation [1]. The exact statistical characterization of a DMC channel requires the solution of this partial differential equation (PDE) with boundary and initial conditions determined by the boundaries of the medium, the receiver and transmitter models, their physical extents and geometries and the chemical reactions in the medium. Hence, the channel model is highly specific to the scenario being considered.

In the literature, analytical characterization of the DMC channel has been investigated for various scenarios. In [2], signal propagation at a tripartite synapse has been modeled. In [3] and [4], a point source within a cylindrical region is considered, modeling microfluidic channels and blood vessels, while [5] and [6] consider point sources within spherical boundaries and transparent receivers, and [7] investigates a spherical transmitter with uniformly distributed ion channels on its surface. The received signal characteristics at a spherical absorbing receiver due to a point transmitter has been derived in [8]. For a thorough account on existing DMC channel models, the reader is referred to [9] and the references therein.

In a practical DMC scenario, there may be physical objects in the medium that interact with the information carrying molecules and interfere with their propagation after release. E.g. obstacles such as cells or debris floating in the medium may interact with the diffusing molecules, or a practical DMC transmitter with a physical extent, such as a bioengineered cell, or a micro-or nanomachine, itself may act as an obstruction to the diffusion after releasing its molecules. Depending on the relative position of the object w.r.t. the release point and the receiver, on the nature of its interaction with the molecules and on its geometry, this will lead to a strengthening or dampening of the received signal, resulting in a directional signal propagation. While [10] and [11] provide simulation based studies on directional transmitters and receivers, respectively, which exploit this phenomenon, no analytical channel model exists in the literature for this practically relevant setting[1].

In this work, we consider the signal propagation in the medium due to a point source located at a distance $d_{TX} \geq 0$ to a spherical object, which may be reflective, partially absorptive or perfectly absorptive. For the first time in the literature, we derive the exact general analytical solution of the PDE for this scenario, which inherently leads to a directional signal propagation pattern. The results obtained from the theoretical analysis allow the statistical characterization of the signal propagation at any arbitrary point in the medium in a variety of practically relevant DMC scenarios including:

Scenario 1: A point source located exactly on the surface of the sphere (i.e. d_{TX}=0). This special case is of paramount practical interest, since it can be employed to model a realistic DMC transmitter with an actual physical extent, which releases molecules from a small opening on its surface, e.g. via exocytosis through a cell membrane, and acts as an obstruction for the diffusing molecules after release[2]. Unlike the ideal isotropic point transmitter model widely employed in the DMC literature, this practical transmitter model inherently results in a directional signal propagation pattern.

Scenario 2: A point source located at an arbitrary distance $d_{TX} > 0$ to a spherical surface. For a perfectly absorbing surface, this model can be employed to determine the temporal and spatial distribution of information carrying molecules that remain unabsorbed in the widely employed point transmitter-absorbing receiver scenario of [8], providing a measure of the directional pattern of possible interference leakage to other DMC systems in the medium. Furthermore, it can be used to model the signal propagation due to a small isotropic source in presence of a large spherical obstacle in the medium.

We validate our analytical results with particle based simulations, and investigate the effect of the system parameters on

Mengüç Öner and Esra Sorguven are with the Dept. of Engineering and Design, University of Sussex, Brighton, UK. e-mail: m.m.oner@sussex.ac.uk, e.sorguven@sussex.ac.uk.

[1]While the signal propagation in [2], [3], [4] and [6] is also directional, it is due to the external boundaries of the medium, and not due to objects within.

[2]While [7] also considers a spherical transmitter with a physical extent, molecules are released from openings uniformly distributed on its surface, which leads to a non-directional signal propagation.

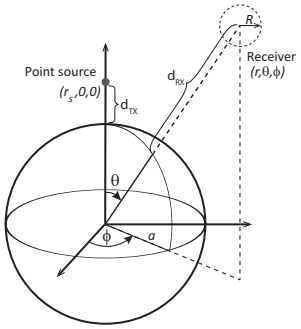

Fig. 1. The system geometry under consideration.

the directivity of the signal propagation pattern in detail for various DMC scenarios of practical interest.

II. System Model and Problem Formulation

We consider an ideal impulsive unit point source over a spherical surface with a radius of a, and a transparent receiver of radius R [9] located at an arbitrary point in the semi-infinite region $r \geq a$ internally bounded by the spherical surface as illustrated in Fig.1. We employ a spherical coordinate system, where r, θ and ϕ represent the radial, elevation and azimuth coordinates respectively, and place the origin at the centre of the sphere. To determine the received signal characteristics given an impulsive release of molecules from the point source at the time instant t_{TX}=0, we consider the time-varying concentration $C(t,r,\theta,\phi)$, which satisfies the diffusion equation:

$$\frac{\partial^2 C}{\partial r^2}+\frac{2}{r}\frac{\partial C}{\partial r}+\frac{1}{r^2\sin\theta}\frac{\partial}{\partial\theta}\left[\sin\theta\frac{\partial C}{\partial\theta}\right]+\frac{1}{r^2\sin^2\theta}\frac{\partial^2 C}{\partial\phi^2}=\frac{1}{D}\frac{\partial C}{\partial t}, \quad (1)$$

where D is the diffusion constant. The initial condition to this PDE imposed by the unit point source can be expressed as:

$$C(t,r,\theta,\phi)|_{t=0}=\frac{\delta(r-r_s)\delta(\theta-\theta_s)\delta(\phi-\phi_s)}{r^2 sin\theta}, \quad (2)$$

where $\delta(\cdot)$ is the Dirac impulse function, and (r_s,θ_s,ϕ_s) are the coordinates of the point source [6]. Without losing generality, the orientation of the coordinate system is chosen in such a way that the point source resides at the coordinates $(r_s,0,0)$, with $r_s = d_{TX}+a$, in order to exploit the symmetry of the problem. The spherical surface may be perfectly reflective, partially absorptive or fully absorptive, which can be modeled by an irreversible ligand-receptor reaction at the surface, leading to the following boundary condition:

$$D\frac{\partial C}{\partial r}\Big|_{r=a}=kC|_{r=a}, \quad (3)$$

where k is the forward reaction constant of the surface reaction. Note that $k=0$ for a perfectly reflective surface, $k\to\infty$ for a perfectly absorptive one and $0<k<\infty$ for a partially absorptive one. Finally, since the medium is externally unbounded

$$C(t,r,\theta,\phi)|_{r\to\infty}=0. \quad (4)$$

While $C(t,r,\theta,\phi)$ represents the concentration distribution in the sense of classical diffusion theory, according to Einstein's theory of diffusion, it can also be interpreted as the time-varying pdf of the position of a single molecule released from the source at $t=0$ [1]. Thus, $P_{obs}(t)$, the probability of observing a molecule at time instant t within a region Ω can be calculated by integrating this expression over Ω. For the transparent receiver with a radius R centered at (r,θ,ϕ), as shown in Fig.1, this integral can be approximated as [6]:

$$P_{obs}(t)=\iiint_{\Omega} C(t,r,\theta,\phi)dv \approx \frac{4\pi R^3}{3}C(t,r,\theta,\phi). \quad (5)$$

Assuming that N_{TX} molecules are released from the source, the number of molecules $N(t)$ received at the transparent receiver can be modeled as a Poisson random variable with an expected value $E\{N(t)\}$=$N_{TX}P_{obs}(t)$ [6]. Thus, the statistical characterisation of the signal propagation requires the solution of the PDE in (1) with the initial- and boundary conditions (2), (3) and (4), which is carried out in the next section.

III. Solution of the PDE

Clearly the problem in Fig.1 is axisymmetric around the axis $\theta=0$, hence $C=C(t,r,\theta)$ i.e. independent of the azimuth angle ϕ. Thus, defining $\mu=cos\theta$, (1) can be simplified as:

$$\frac{\partial^2 C}{\partial r^2}+\frac{2}{r}\frac{\partial C}{\partial r}+\frac{1}{r^2}\frac{\partial}{\partial\mu}\left[(1-\mu^2)\frac{\partial C}{\partial\mu}\right]=\frac{1}{D}\frac{\partial C}{\partial t} \quad (6)$$

A common technique for solving such a PDE is to split C into two terms, $C=U+V$, where V is a solution satisfying the initial condition due to the point source and U is a solution that vanishes at $t=0$. In [12], it has been shown that

$$V=\frac{1}{(4\pi Dt)^{3/2}}e^{-\frac{r^2-2\mu r r_s+r_s^2}{4Dt}} \quad (7)$$

satisfies the initial conditions due to the point source. A solution for U can be found by substituting it in (6) and taking the Laplace transform. Since U vanishes at $t=0$,

$$\frac{\partial^2\tilde{U}}{\partial r^2}+\frac{2}{r}\frac{\partial\tilde{U}}{\partial r}+\frac{1}{r^2}\frac{\partial}{\partial\mu}\left[(1-\mu^2)\frac{\partial\tilde{U}}{\partial\mu}\right]-\lambda^2\tilde{U}=0, \quad (8)$$

where $\tilde{U}$ is the Laplace Transform of U and $\lambda=\sqrt{s/D}$. Equation (8) can be solved by employing Separation of Variables [13]. Substituting $\tilde{U}(r,\mu)=G(r)H(\mu)$ in (8) we get:

$$\frac{r^2}{G}\frac{\partial^2 G}{\partial r^2}+\frac{2r}{G}\frac{\partial G}{\partial r}-\lambda^2 r^2=-\frac{1}{H}\frac{\partial}{\partial\mu}\left[(1-\mu^2)\frac{\partial H}{\partial\mu}\right] \quad (9)$$

Clearly (9) can only be satisfied if both sides of the equation are equal to a constant. Choosing the separation constant as $n(n+1)$ for integer n leads to:

$$\frac{\partial}{\partial\mu}\left[(1-\mu^2)\frac{\partial H}{\partial\mu}\right]+n(n+1)H=0, \quad (10)$$

$$\frac{\partial^2 G}{\partial r^2}+\frac{2}{r}\frac{\partial G}{\partial r}-\left(\lambda^2+\frac{n(n+1)}{r^2}\right)G=0. \quad (11)$$

The principle solutions to Eq. (10) are $P_n(\mu)$ and $Q_n(\mu)$, i.e. Legendre functions of the first and second kind of order n [13], whereas the principle solutions to (11) are $\frac{1}{\sqrt{r}}I_{n+1/2}(\lambda r)$ and $\frac{1}{\sqrt{r}}K_{n+1/2}(\lambda r)$ where $I_\nu(\cdot)$ and $K_\nu(\cdot)$ are modified Bessel functions of the first and second kind, respectively, of order ν [13]. Note that $Q_n(\mu)$ diverge for $\mu\to\pm1$ (i.e. $\theta\to0$ and π), similarly $\frac{1}{\sqrt{r}}I_{n+1/2}(\lambda r)$ approach ∞ as $r\to\infty$ and cannot satisfy (4). Thus the solution to $\tilde{U}$ is in the form

$$\tilde{U}=\sum_{n=0}^{\infty}\beta_n\frac{1}{\sqrt{r}}K_{n+\frac{1}{2}}(\lambda r)P_n(\mu). \quad (12)$$

The coefficients β_n are determined by applying the boundary condition in (3) to the total solution in Laplace domain. Laplace transforming (7) yields, with $\rho=\sqrt{r^2-2\mu r r_s+r_s^2}$:

$$\tilde{V}=\frac{e^{-\lambda\rho}}{4\pi D\rho}=\frac{1}{4\pi D}\sum_{n=0}^{\infty}\frac{2n+1}{\sqrt{rr_s}}P_n(\mu)I_{n+\frac{1}{2}}(\lambda r)K_{n+\frac{1}{2}}(\lambda r_s) \quad (13)$$

where $\tilde{V}$ is the Laplace Transform of V. The first equality in (13) can be found in Laplace Transform tables, and the infinite sum representation in the second equality is found in [14]. Adding (12) to (13) leads to the solution $\tilde{C}=\tilde{U}+\tilde{V}$ in Laplace domain:

$$\tilde{C}=\sum_{n=0}^{\infty}\frac{P_n(\mu)}{\sqrt{r}}\left(\frac{2n+1}{4\pi D\sqrt{r_s}}I_{n+\frac{1}{2}}(\lambda r)K_{n+\frac{1}{2}}(\lambda r_s)+\beta_n K_{n+\frac{1}{2}}(\lambda r)\right). \quad (14)$$

The coefficients β_n are determined by applying the boundary condition (3) to (14) which leads to:

$$\beta_n=-\frac{2n+1}{4\pi D\sqrt{r_s}}K_{n+\frac{1}{2}}(\lambda r_s)\frac{2\lambda a I'_{n+\frac{1}{2}}(\lambda a)-(\frac{2ka}{D}+1)I_{n+\frac{1}{2}}(\lambda a)}{2\lambda a K'_{n+\frac{1}{2}}(\lambda a)-(\frac{2ka}{D}+1)K_{n+\frac{1}{2}}(\lambda a)} \quad (15)$$

where $'$ denotes the derivative operation. The concentration in time domain is obtained by substituting (15) in (14) and taking the inverse Laplace transform, $C=\mathcal{L}^{-1}\{\tilde{C}\}$. Since there is no readily available inverse transform for the resulting expression, we make use of the inversion theorem, which leads to:

$$C=\sum_{n=0}^{\infty}\frac{2n+1}{\sqrt{rr_s}}P_n(\mu)\frac{1}{2\pi j}\int_{\sigma-j\infty}^{\sigma+j\infty}\tilde{\Gamma}_n(\lambda,r)e^{st}ds. \quad (16)$$

where $\tilde{\Gamma}_n(\lambda,r)$ is given in Eq. (17) at the bottom of this page, with $\lambda=\sqrt{s/D}$. Note that the integrand in (16) has a branch cut on $s\in(-\infty,0]$, and no poles on the complex plane. Employing usual contour integration techniques, the integral over the complex path in (16) can be expressed as the sum of two integrals over the negative real line, one corresponding to the path just over the branch cut, and the other to the path just underneath. After appropriate simplifications, we get

$$C=\sum_{n=0}^{\infty}\frac{2n+1}{\sqrt{rr_s}}P_n(\mu)\frac{1}{\pi}\int_0^{\infty}\mathcal{I}m\{\tilde{\Gamma}_n(j\gamma,r)\}e^{-D\gamma^2 t}\gamma d\gamma, \quad (18)$$

where $s=-\gamma^2 D$, $\gamma\in\mathbb{R}$ and $\mathcal{I}m\{\cdot\}$ is the imaginary part. Eq. (18) with (17) can be simplified by expressing the modified Bessel functions with purely imaginary arguments in terms of Bessel functions with real valued arguments [14], which finally leads to the complete and exact solution of the PDE given in Eq. (19), the second equation at the bottom of this page, where

$$A_\nu(\gamma,r)=J_\nu(\gamma r)Y'_\nu(\gamma a)-Y_\nu(\gamma r)J'_\nu(\gamma a), \quad (20)$$

$$B_\nu(\gamma,r)=J_\nu(\gamma r)Y_\nu(\gamma a)-Y_\nu(\gamma r)J_\nu(\gamma a), \quad (21)$$

and $J_\nu(\cdot)$ and $Y_\nu(\cdot)$ are the Bessel functions of the first and second kind, respectively, of order ν. The following observations can be made from Eq. (19):

1) Eq. (19) expresses the time varying concentration at any point in the region bounded internally by the spherical surface. The solution is in the form of an infinite sum of real valued integrals depending on r that are weighted by coefficients depending on $\mu=cos(\theta)$, which results in a directional signal propagation with the axis $\theta=0$ the main direction of propagation maximizing C. While no closed form expression exists for the integrals involving the Bessel functions, they can be evaluated using numerical methods.

*2)*The special case of a perfectly reflective surface can be accommodated by substituting $k=0$ in (19). In the special case of a perfectly absorbing surface, $k\to\infty$, which leads to:

$$C(t,r,\mu)=\sum_{n=0}^{\infty}\frac{2n+1}{4\pi\sqrt{rr_s}}P_n(\mu)\int_0^{\infty}\frac{B_{n+\frac{1}{2}}(\gamma,r)B_{n+\frac{1}{2}}(\gamma,r_s)}{J^2_{n+\frac{1}{2}}(\gamma a)+Y^2_{n+\frac{1}{2}}(\gamma a)}e^{-D\gamma^2 t}\gamma d\gamma. \quad (22)$$

3) It is not the reaction coefficient k alone that determines if absorption or reflection is more prevalent in the signal propagation, but rather the ratio $2ka/D$. If $2ka\gg D$, absorption dominates, (19) converges to (22), and the spherical surface acts as almost perfectly absorbing. In contrast, if $2ka\ll D$, the surface acts as almost purely reflective.

4) The concentration function, and consequently, the corresponding DMC channel, exhibit a reciprocal behaviour, i.e. the value of C remains the same if the location of the observation point (r,θ,ϕ) (the receiver's center), and the location of the point source are interchanged [6]. Thus, in principle, a configuration that results in a directional transmitter can be transformed into a directional receiver (see [11]) by exchanging the positions of the point source and the observation point.

5) The infinite sum in (19) converges rapidly, hence, it is sufficient to evaluate only its first few terms for accurately computing C, which will be demonstrated in the next section.

IV. Results

In this section, the results obtained from our theoretical analysis are validated with particle based simulations (PBS), and the directivity of the signal propagation is investigated in DMC scenarios of practical interest. For all the provided results, the diffusion constant has been chosen as $D=10^{-9}m^2s^{-1}$, and a transparent receiver of radius $R=1\mu m$ is considered. The PBSs have been carried out with the particle based DMC simulator AcCoRD v1.4.2 [15], with a diffusion timestep of $2\mu s$ in the time interval $0\le t\le 20ms$, where $N_{TX}=1.6\times10^5$ molecules are released at each iteration and 1000 iterations are performed for each case. The theoretical results for P_{obs} are computed by evaluating (19) or (22), truncating the summation at $n=5$ and using the approximation in Eq.(5). Throughout

$$\tilde{\Gamma}_n(\lambda,r)=K_{n+\frac{1}{2}}(\lambda r_s)\frac{I_{n+\frac{1}{2}}(\lambda r)\left[2\lambda a K'_{n+\frac{1}{2}}(\lambda a)-(\frac{2ka}{D}+1)K_{n+\frac{1}{2}}(\lambda a)\right]-K_{n+\frac{1}{2}}(\lambda r)\left[2\lambda a I'_{n+\frac{1}{2}}(\lambda a)-(\frac{2ka}{D}+1)I_{n+\frac{1}{2}}(\lambda a)\right]}{2\lambda a K'_{n+\frac{1}{2}}(\lambda a)-(\frac{2ka}{D}+1)K_{n+\frac{1}{2}}(\lambda a)} \quad (17)$$

$$C(t,r,\mu)=\sum_{n=0}^{\infty}\frac{2n+1}{4\pi\sqrt{rr_s}}P_n(\mu)\int_0^{\infty}\frac{\left[2\gamma a A_{n+\frac{1}{2}}(\gamma,r)-(\frac{2ka}{D}+1)B_{n+\frac{1}{2}}(\gamma,r)\right]\left[2\gamma a A_{n+\frac{1}{2}}(\gamma,r_s)-(\frac{2ka}{D}+1)B_{n+\frac{1}{2}}(\gamma,r_s)\right]}{[2\gamma a J'_{n+\frac{1}{2}}(\gamma a)-(\frac{2ka}{D}+1)J_{n+\frac{1}{2}}(\gamma a)]^2+[2\gamma a Y'_{n+\frac{1}{2}}(\gamma a)-(\frac{2ka}{D}+1)Y_{n+\frac{1}{2}}(\gamma a)]^2}e^{-D\gamma^2 t}\gamma d\gamma. \quad (19)$$

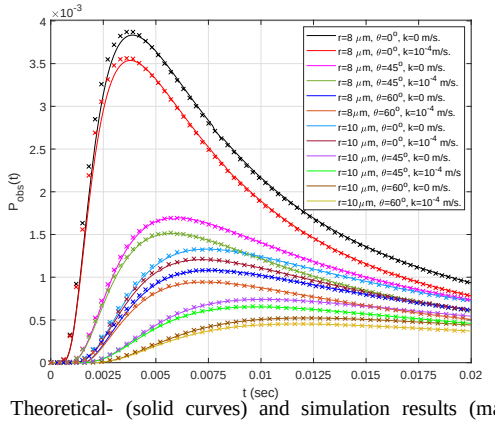

Fig. 2. Theoretical- (solid curves) and simulation results (markers) for $P_{obs}(t)$ for a sphere with a point source exactly on the surface ($r_s{=}a{=}3\mu m$), at various values of θ and r, $k{=}0$ and $10^{-4}m/s$, $d_{RX} = 5, 7\mu m$.

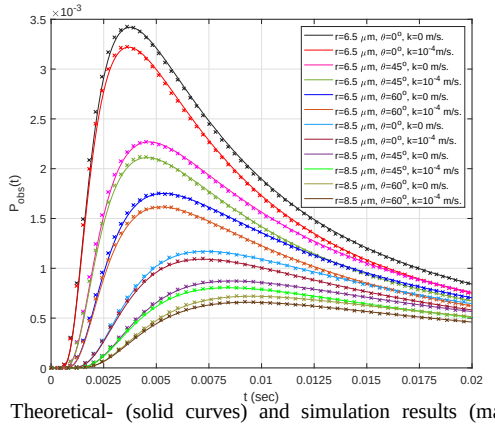

Fig. 3. Theoretical- (solid curves) and simulation results (markers) for $P_{obs}(t)$ for a sphere with a point source exactly on the surface ($r_s{=}a{=}1.5\mu m$), at various values of θ and r, $k{=}0$ and $10^{-4}m/s$, $d_{RX} = 5, 7\mu m$.

the Figs 2 to 4, the theoretical results are represented with solid curves, and the corresponding PBS results with markers of the same color.

Figures 2 and 3 display the results obtained both from our theoretical analysis (solid curves) and PBSs (markers) for a spherical surface with the point source located exactly on the surface ($r_s = a$), modeling a realistic DMC transmitter as described in the Scenario 1 of Section I, for $a = 3$ and $1.5\mu m$ respectively. In order to ensure a fair comparison of signal strength between these two cases, we choose the values of r in both cases such that the receiver-to-surface distances $d_{RX}{=}r-a$ remain the same as a changes. Both the case of a perfectly reflective surface ($k{=}0$) and a partially absorbing surface ($k = 10^{-4}m/s$) are considered and P_{obs} is evaluated for various values of θ. Clearly the results obtained from the theoretical analysis and simulations are in excellent agreement. The presence of absorption at the surface leads to a decrease in $P_{obs}(t)$ compared to the perfectly reflective case. Furthermore, the directional variation of the signal strength is more prevalent for $a{=}3\mu m$ compared to the case where $a{=}1.5\mu m$.

Fig. 4 investigates the Scenario 2 of Section I where the spherical surface is perfectly absorptive ($k \to \infty$) and the point source is located $d_{TX} = 2\mu m$ above it. $P_{obs}(t)$ is evaluated for $a = 1.5$ and $3\mu m$, $d_{RX}{=}9$ and $10\mu m$ and 3 values of θ. Once more, the theoretical results and simulations are in very

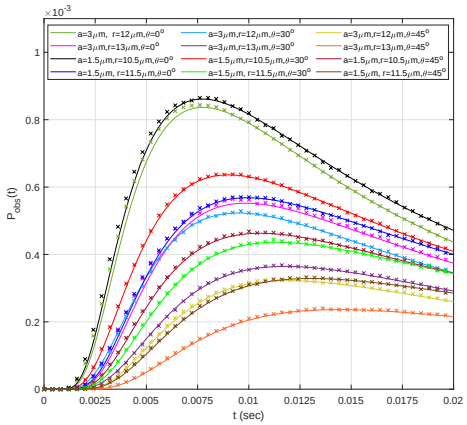

Fig. 4. $P_{obs}(t)$ for a perfectly absorbing sphere ($a = 3, 1.5\mu m$) with a point source $d_{TX}{=}2\mu m$ above it, for various values of θ and r.

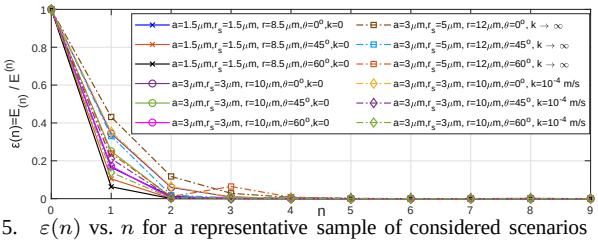

Fig. 5. $\varepsilon(n)$ vs. n for a representative sample of considered scenarios

good agreement, validating our theoretical analysis.

As stated previously, the infinite sum in (19) converges rapidly, and, in our analytical results, we truncate this sum after $n = 5$. Let $E_{(n)}$ be the energy of the n'th term of the sum in (19) at a given point, and $E^{(n)}$ be the energy of the total sum truncated after the n'th term. Then $\varepsilon(n) = E_{(n)}/E^{(n)}$ provides a measure of the relative energy of the final term of the sum to the energy of the truncated sum as a function of n, and shows how rapidly the sum converges. For all the cases considered in this work, a representative sample of which has been displayed in Fig. 5, we observe a very rapid drop of $\varepsilon(n)$ with increasing n, and a convergence to practically 0 at around $n = 5$. This, and the remarkable agreement between the theory and simulations seen in Figs. 2 to 4 provide sufficient justification for our choice of truncating (19) at $n = 5$, and further validation for our theoretical results.

In order to quantify the directionality of the expected signal strength at a given distance r, we consider $P_{obs}(t_{max})$ where t_{max} is the time instant where P_{obs} attains its maximum in the direction of maximum directivity ($\theta = 0$). Fig. 6 illustrates this directionality for three cases of practical interest by using the analytical solution in (19). Fig. 6(a) examines the Scenario 1 of Section I, where the point source is exactly on a reflective surface ($r_s{=}a$), and investigates the effect of its radius a on the directionality of the signal propagation pattern. To provide a fair comparison of signal amplitudes between cases with different radii a, we keep $d_{RX} = r - a$ constant at $7\mu m$. Clearly, the signal propagation pattern exhibits a considerable directionality which increases with a, becoming narrower and increasing in amplitude towards the main axis of propagation. Fig. 6(b) illustrates the same scenario with a partially absorbing spherical surface, and investigates the effect

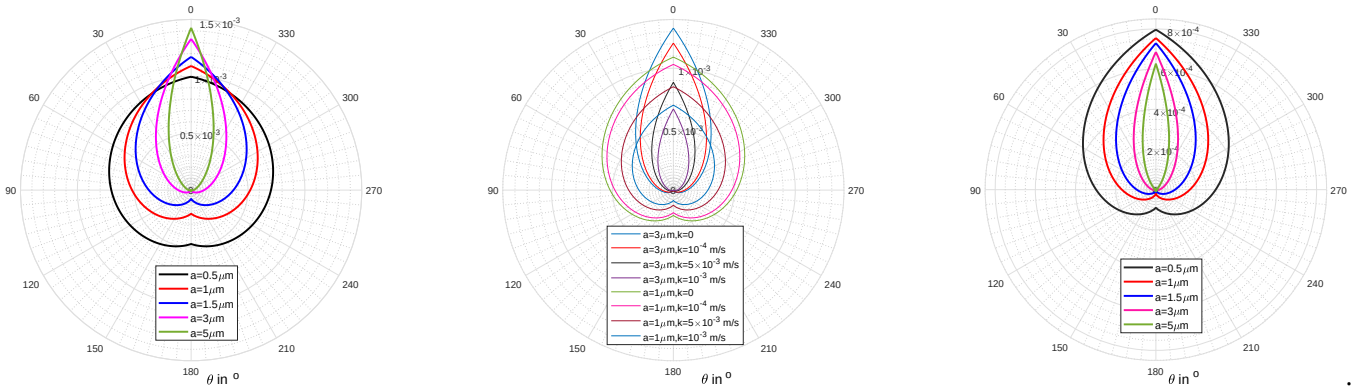

(a) $r_s = a$, $d_{RX} = r - a = 7\mu m$, $k = 0$. (b) $r_s = a$, $d_{RX} = r - a = 7\mu m$. (c) $d_{TX} = 1\mu m$, $r - r_s = 7\mu m$, $k \to \infty$.

Fig. 6. Directional signal propagation patterns $P_{obs}(t_{max})$ for scenarios of practical interest: (a) A perfectly reflective sphere with a point source exactly on the surface ($r_s = a$) for various values of a. (b) Effect of the surface reaction coefficient k on the signal propagation pattern for a point source exactly on the spherical surface ($r_s = a$). (c) A perfectly absorbing sphere with a point transmitter $d_{TX} = 1\mu m$ above the surface, $r - r_s = 7\mu m$, for various values of a.

of the reaction coefficient k on the propagation pattern. As expected, the increase in k has no effect on the shape of the propagation pattern, and only leads to a uniform decrease in the signal amplitude over all values of θ, since the absorption takes place uniformly over the surface. Finally, Fig. 6(c) displays the propagation pattern for a perfectly absorbing sphere with a point transmitter d_{TX}=$1\mu m$ above the surface, as described in Scenario 2, for different values of a. To provide a fair comparison while varying a, we keep $r - r_s$ constant at $7\mu m$. Here, similar to Fig. 6(a), the propagation pattern becomes more directional as a increases, however, in contrast to Fig. 6(a), the amplitude decreases with increasing a due to the increase of the surface area of the perfectly absorbing sphere. Both Figs 6(a) and (c), and further results that couldn't be displayed here due to space limitations, indicate that the relation between the transmission distance and the radius a is a determining factor in the directivity of the signal propagation. For $r \gg a$, the propagation pattern converges to that of an isotropic source.

V. Conclusion

This work investigates the temporal and spatial signal propagation in DMC due to a point source located at a distance $d_{TX} \geq 0$ to a spherical surface which may be reflective, partially absorptive or fully absorptive. The analytical solution of the resulting PDE has been derived and validated by particle based simulations, which shows a directional signal propagation characteristics. The result obtained by our theoretical analysis is general and can be evaluated using numerical integration. A close inspection of the analytical result reveals that this DMC channel is reciprocal. The system model investigated in this work can be employed to determine the signal propagation characteristics in a variety of DMC scenarios of considerable practical interest, for which the effect of system parameters on the propagation pattern has been examined in detail. Our future research will include the extension of the signal propagation analysis in this work to scenarios with absorbing receiver models.

References

[1] D. Gillespie and E. Seitaridou, *Simple Brownian Diffusion: An Introduction to the Standard Theoretical Models.* Oxford Univ. Press, 2013.

[2] S. Lotter, A. Ahmadzadeh, and R. Schober, "Synaptic channel modeling for dmc: Neurotransmitter uptake and spillover in the tripartite synapse," *IEEE Trans. Commun.*, vol. 69, no. 3, pp. 1462–1479, 2021.

[3] M. Zoofaghari and H. Arjmandi, "Diffusive molecular communication in biological cylindrical environment," *IEEE Trans. Nanobiosci.*, vol. 18, no. 1, pp. 74–83, 2019.

[4] F. Dinc, B. C. Akdeniz, A. E. Pusane, and T. Tugcu, "A general analytical approximation to impulse response of 3-d microfluidic channels in molecular communication," *IEEE Trans. Nanobiosci.*, vol. 18, no. 3, pp. 396–403, 2019.

[5] X. Bao, Y. Zhu, and W. Zhang, "Channel characteristics for molecular communication via diffusion with a spherical boundary," *IEEE Wireless Commun. Lett.*, vol. 8, no. 3, pp. 957–960, 2019.

[6] H. Arjmandi, M. Zoofaghari, and A. Noel, "Diffusive molecular communication in a biological spherical environment with partially absorbing boundary," *IEEE Trans. Commun.*, vol. 67, no. 10, pp. 6858–6867, 2019.

[7] H. Arjmandi, A. Ahmadzadeh, R. Schober, and M. Nasiri Kenari, "Ion channel based bio-synthetic modulator for diffusive molecular communication," *IEEE Trans. Nanobiosci.*, vol. 15, no. 5, pp. 418–432, 2016.

[8] H. B. Yilmaz, A. C. Heren, T. Tugcu, and C. Chae, "Three-dimensional channel characteristics for molecular communications with an absorbing receiver," *IEEE Commun. Lett.*, vol. 18, no. 6, pp. 929–932, 2014.

[9] V. Jamali, A. Ahmadzadeh, W. Wicke, A. Noel, and R. Schober, "Channel modeling for diffusive molecular communication—a tutorial review," *Proceedings of the IEEE*, vol. 107, no. 7, pp. 1256–1301, 2019.

[10] H. B. Yilmaz, G. Suk, and C. Chae, "Chemical propagation pattern for molecular communications," *IEEE Wireless Commun. Lett.*, vol. 6, no. 2, pp. 226–229, 2017.

[11] L. Felicetti, M. Femminella, and G. Reali, "Directional receivers for diffusion-based molecular communications," *IEEE Access*, vol. 7, pp. 5769–5783, 2019.

[12] A. Haji Sheikh, K. Cole, J. Beck, and B. Litkouhi, *Heat Conduction Using Green's Functions*. CRC Press, 2010.

[13] M. Willatzen and L. C. L. Yan Voon, *Separable Boundary-Value Problems in Physics*. John Wiley and Sons, Ltd, 2011.

[14] G. N. Watson, *A Treatise on the Theory of Bessel Functions, 2nd Edition*. Cambridge Univ. Press, 1944.

[15] A. Noel, K. C. Cheung, R. Schober, D. Makrakis, and A. Hafid, "Simulating with accord: Actor-based communication via reaction–diffusion," *Nano Commun. Netw.*, vol. 11, pp. 44 – 75, 2017.